Comparative study between transverse and longitudinal acoustic modes on a premixed V-shape flame

M. Cáceres*, F. Baillot, F. Lespinasse, E. Domingues

CORIA, UMR 6614, CNRS, Experimental Combustion

Abstract

This work compares the effects on an inverted conical premixed flame and its incoming annular jet, of a longitudinal mode induced by a transverse standing acoustic field with those of a direct longitudinal acoustic mode. The dynamic responses of the fluid system are investigated by means of optical diagnostics and pressure measurements. A fine analysis of the jet properties dynamics (velocity, vorticity, vortical structures...) and flame characteristics (CH* emission, front wrinkling…) demonstrate that the longitudinal acoustic mode induced by the transverse one is identical to the direct longitudinal acoustic mode.

Introduction

From the beginning of combustion system designs, identify and understand instabilities related to combustion process have always been a priority. Some works have classified them according to their origins. One source of instabilities relies on the geometry of the chamber where the combustion noise can induce strong pressure oscillations exciting one or several of its resonant modes. Once pressure fluctuations coupled with heat release rate modulations, thermo-acoustic instabilities can grow. Their amplification can diminish energy efficiency and even destroy the combustor.

The position of the reactant jet injection inside the chamber is linked to the chamber acoustic modes. Fig. 1a shows a longitudinal mode propagating in the injection direction and transverse standing modes perpendicular to it. In axisymmetric combustors (Fig.1b), azimuthal modes perpendicular to the injectors can be spinning or standing while radial modes are necessarily standing. In practice these latter ones involving very high frequencies are difficult to be excited.

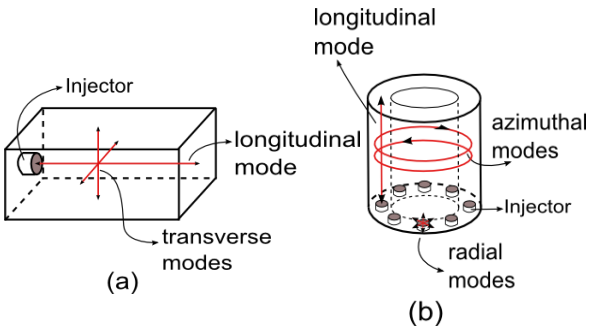

Fig. 1. Chamber: (a) right section, (b) annular section

Thermoacoustic instability feedback: flames, due to variations of its surface and of its heat release rate are a source of acoustic waves. The direct combustion noise may feed the resonant chamber modes whose acoustic energy can be enhanced via the Rayleigh criterion. Likewise the acoustic modes can give rise to flow perturbations causing the variation of some of its dynamic properties. In their turn, these ones modify the flames' surface and their heat release rate, closing the thermo-acoustic coupling loops (Fig. 2), provided that the Rayleigh source term is high enough to counterbalance any stabilizing quantity as the damping.

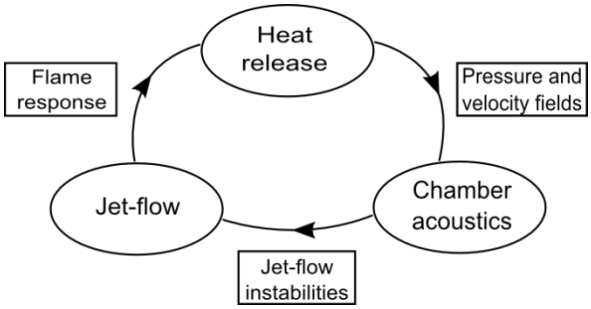

Fig. 2. Thermo-acoustic coupling loop

Main objective

Some experimental works (e.g. [1, 2, 3]) and numerical simulations (e.g.[4]) highlighted a mode conversion from the transverse wave set in a combustion cavity to a longitudinal wave developing along the reactant injector system, a phenomenon knew as "injector coupling" [5]. The induced longitudinal mode can drive flow perturbations, including those activating jet instabilities, which form vortices able to modify flame dynamics (Fig. 3a). Herein the flow perturbations are the main source of flame surface modulations and of periodic flame foot displacement, which causes the heat release rate to fluctuate [1, 6].

By means of a fine analysis of both jet and flame dynamics, this work aims to answer the following question: is the longitudinal mode induced by a standing wave the same as a direct longitudinal mode (Fig. 3b)? Up to now, no studies to our knowledge have investigated these two kinds of longitudinal modes in order to compare them via a systematic analysis of their properties and to conclude on their equivalence.

Experimental facility

The set-up (Fig. 4) is that of a previous study [1, 6, 8].

Fluid system without acoustics: The cylindrical burner is composed of three main parts: an upstream tube, 135 mm long with internal diameter of 65 mm, a converging profiled unit, 59 mm long with an internal diameter decreasing from 65 to 22 mm, and a conver-

* Corresponding author: marcos.caceres@coria.fr

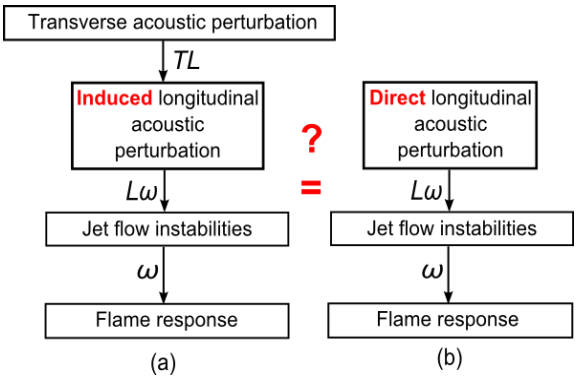

Fig. 3. Mechanisms acting on flames via: (a) induced longitudinal perturbations, (b) direct longitudinal perturbations.

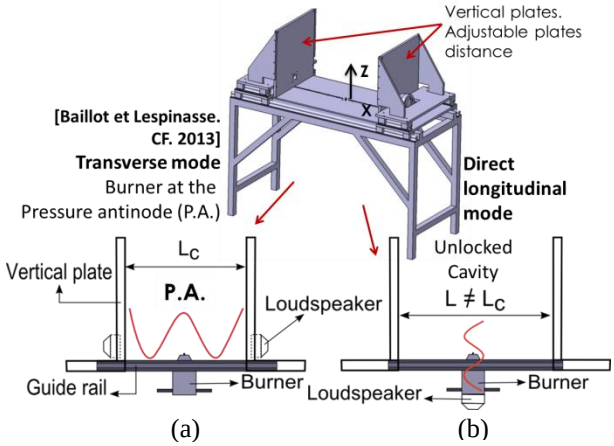

Fig. 4. Acoustic set-up: (a) standing transverse mode generation; (b) longitudinal mode generation.

gent nozzle with a 10 mm exit diameter (D). A central rod is introduced inside the burner and aligned with its axis. The rod diameter d_r is 3 mm. Its extremity stands out by $l_r = 3{,}5\ mm$ above the burner exit. Flames issue from a methane-air premixing. The mass flow rate of each gas is measured by Teledyne Hastings flow-meter.

The fluid system (jet-flow and flame) is naturally axisymmetric (Fig. 5). The laminar jet stabilizes a laminar V-shape flame above the rod. Two boundary layers are identified: the outer one with the surrounding air and the inner one at the rear of the rod. The flow rate velocity is $U_{bulk} = 2.1$ m/s, and the equivalence ratio $\phi = 1$. Measurements are specified in the Cartesian coordinate system (O, x, y, z) where O is located in the middle of the burner exit cross-section (see Fig. 5).

Transverse standing acoustic field: It is composed of a steel semi-open acoustic cavity. The two vertical opposite walls are steel plates (Fig. 4), in each of them a Beyma driver unit is implemented. The distance L_c between the plates is variable in order that the first resonant mode of the cavity can be excited for any studied frequency f_0 ranging from 500 to 1200 Hz (Fig 4a). The burner is fixed in the middle of the cavity bottom. The plates can slide together to place the burner at any position inside the acoustic field generated by the driver units. Here the burner has been always kept at the pressure antinode where the mode transfer mechanism is at its maximum efficiency and undisturbed by any other phenomena that may be present in the other locations of the acoustic field. The whole acoustic field was characterized in [6] and extended descriptions are in [8].

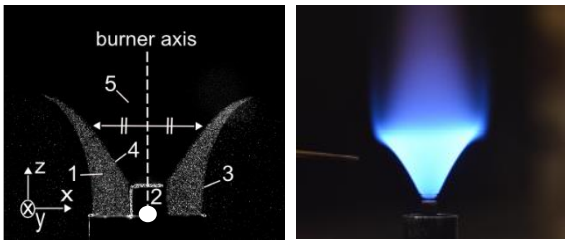

Fig. 5. Fluid system without acoustics. Laser tomography visualization (left): seeded jet (**1**), stabilization rod (**2**), shear layers: outer (**3**) and inner (**4**), burnt gases (**5**), white point: origin of the Cartesian frame of reference O ($x = 0, y = 0, z = 0$). Premixed V-flame (right).

Direct longitudinal acoustic field: In Fig. 4b a loudspeaker is mounted at the bottom of the burner in order to generate a longitudinal acoustic mode in the jet-flow direction. The plates are unlocked and separated enough from each other to avoid the creation of a standing transverse acoustic wave. Measurements of the pressure field around the burner exit show that it is evanescent due to sound radiation.

Methodology

The jet dynamics has been studied by means of a phase-locking technique using PIV and pressure measurements. A dual pulse Nd: YAG laser is used with a double frame Image Pro X 4M camera equipped with a 180-mm Nikon lens ($f/2.8$). The time between two pulses is set to 30 μs and the spatial resolution is about 78 pixels/mm. Velocities are calculated through a three-pass operation: interrogation windows sizes are from 128×128 pixels to 32×32 pixels, with an overlap of 50%. Pressure fluctuations are recorded by a microphone B&K Model 4182 with a $1\ \text{Hz} - 20\ \text{KHz}$ frequency response, placed in the burner vicinity ($x = 10\ \text{mm}, y = 10\ \text{mm}, z = 10\ \text{mm}$). There the pressure fluctuations are noted $P'_{ref}(t)$ and their amplitude is $\tilde{P}_{ref}$. The premixing has been seeded by olive oil droplets used as scattering particles. For PIV the whole cavity is seeded by smoke fluid particles simultaneously to the jet seeding. The overall CH* emission is recorded by a photomultiplier (PM) Hamamatsu H6779 positioned 40 cm away from the flame in order to collect all the CH* light emitted by the flame (I_{CH^*}). The PM is fitted with an interferential filter centered at $\lambda = 430$ nm with a full width at half maximum $\Delta\lambda = 10$ nm ± 2 nm. It is known that I_{CH^*} is proportional to the global heat release rate at stoichiometry. The jet and flame visualization is ensured by laser tomography technique using the same camera as that for PIV. Thus, the cycle of the fluid system is reconstructed by phase-locking images.

Choice of the operating conditions

In this work, the operating conditions used in the transverse mode configuration have been chosen from the flame response chart established in [1] and reported in Fig. 6. It gathers the various types of flame behaviors in the physical space ($St,\ \tilde{P}_{ref}/\tilde{P}_{bo}$). The ratio $\tilde{P}_{ref}/\tilde{P}_{bo}$ is defined as the amplitude of a current pressure signal over $\tilde{P}_{bo}$ the amplitude corresponding to the flame blowout. The Strouhal number is given by $St_D = f_0 D/U_{bulk}$ or $St_{dr} = f_0 d_r/U_{bulk}$ according to which boundary layer (inner or outer) preferentially drives the flame response. Whatever the conditions chosen in that chart, the comparative analysis between the two acoustic configurations, induced and direct longitudinal modes, leads to the same conclusions. So the condition labeled A in Fig. 6 is chosen to illustrate the present work. In addition, two other conditions B and C are used for specific points. A, B and C correspond to the following responses detailed in [1]. A is a "strongly rolled-up flame", described by a frequency bifurcation in the fluid system response such that the action of outer vortices, piloted by a sub-harmonic process at $f_0/2$, is dominant; B is a "strongly rolled-up flame" equally sensitive to outer vortices driven by $f_0/2$ and inner vortices driven by f_0, such that a competition appears between the two modes; and C is an "elongated wrinkled flame" driven by the inner layer at f_0. These cases situated near to blowout are significant to strongly disturbed flame dynamics [1, 8].

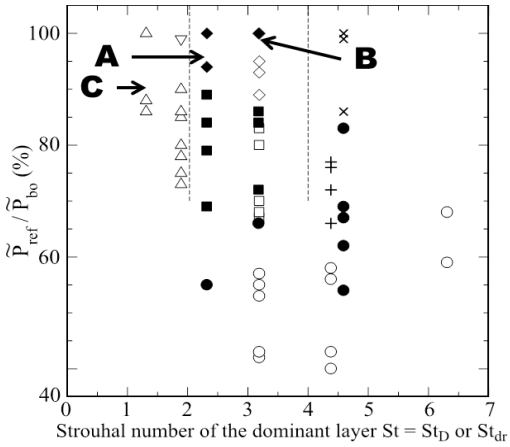

Fig. 6. Points **A**, **B** and **C** in the flame response chart [1]. Symbols depending on the peak frequency f_f of I_{CH^*} signal defined as the dominant flame frequency in the physical space ($St,\ \tilde{P}_{ref}/\tilde{P}_{bo}$); open symbols: $U_{bulk} = 1.6$ m/s; filled symbols: $U_{bulk} = 2.2$ m/s

Spatially averaged vertical velocity U_p^*

The velocity U_p^* results from the spatial average of velocities U'_p measured along an annular radius r at the burner exit ($z_0 = 0.21$ mm) from a series of N PIV-images recorded at a given locked phase (t_i) (eq. 1). Here $N = 100$ and ten phases are chosen to reconstruct an overall cycle.

$$U_p^*(t_i) = \frac{\sum_N U_p(t_i)}{N}, \text{ with } U_p(t_i) = \frac{\int_{d_r/2}^{D/2} U'_p r dr}{(D/2)^2 - (d_r/2)^2} \quad (1)$$

The signals U_p^* calculated in the induced and direct longitudinal modes configurations are synchronized via a common initial phase time t_0. This time corresponds to the instant at which a vortex generated by one of the acoustic fields is visualized as it is ejected at the burner exit. The acoustic pressure amplitudes $\tilde{P}_{ref}$ of the two configurations are adjusted to obtain the same amplitude

Table 1. $\tilde{P}_{ref}$ and $\tilde{P}_{ref}/\tilde{P}_{bo}$ values for 3 frequencies representative of those found in practical devices. A, B and C: cases in Fig. 6.

$\tilde{P}_{ref}$ [Pa] for the same $U_p^*(t_i)$ evolution over time			
Forcing frequency f_0	Direct longitudinal mode	Induced longitudinal mode	$\tilde{P}_{ref}/\tilde{P}_{bo}$
510 Hz (A)	3.4	180	≈ 0.97
700 Hz (B)	6.7	370	≈ 0.98
1010 Hz (C)	10.5	350	≈ 0.91

for U_p^*. $\tilde{P}_{ref}$ are quite different in the two cases as illustrated in Table 1. Indeed, depending on f_0, the amplitude of the transverse wave is ranging from 180 to 370 Pa whereas that of the direct longitudinal wave varies from 3 to 10 Pa. But *a posteriori* $\tilde{P}_{ref}/\tilde{P}_{bo}$ is verified to be the same in both configurations. Such an example reporting U_p^* as a function of t_i during a reconstructed cycle for each mode configuration is presented in Fig. 7.

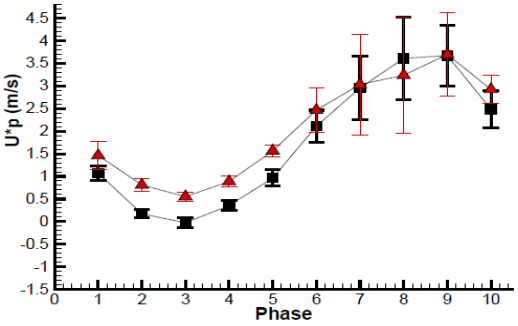

Fig. 7. Velocity U_p^* with error bars. Case A. ■ Longitudinal forcing; ▲ transverse forcing.

Jet acceleration γ_p^*

The global jet acceleration is calculated from the velocity $U_p^*(t_i)$. Depending on the type of longitudinal modes, the acceleration evolves differently with the pressure fluctuations. With the transverse wave, when the pressure oscillation amplitude is growing (diminishing), the jet is compressed and decelerated (expanded and accelerated). This feature is recognized as a plugging effect [1, 6]. The acoustic pressure and jet acceleration are globally out-of-phase, as illustrated in Fig. 8.

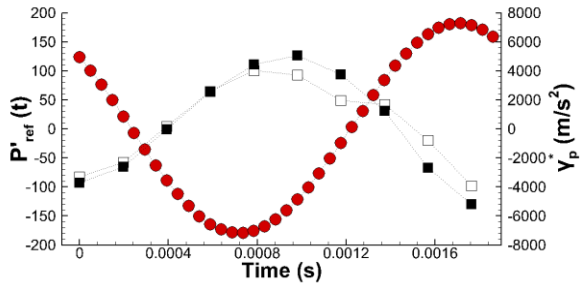

Fig. 8. Acoustic pressure of the transverse wave: $P'_{ref}(t)$ (●); perturbed flow acceleration γ_p^*: (□) left side; (■) right side. Case A

For the direct longitudinal mode, in all the cases, the pressure oscillation imposes a pumping effect on the jet-flow: when the pressure amplitude is growing (diminishing), the jet is pushed out (pulled in) and accelerated (decelerated). The pressure and jet acceleration are globally in-phase (Fig. 9).

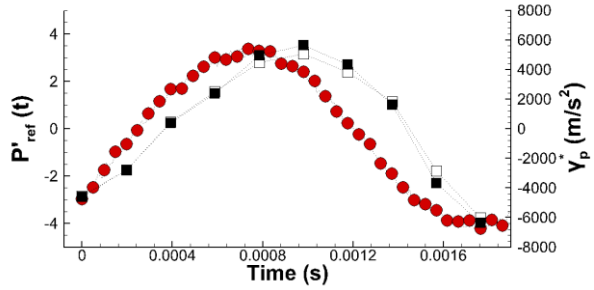

Fig. 9. Acoustic pressure of the direct longitudinal mode corresponding to case A: $P'_{ref}(t)$ (●); perturbed flow acceleration γ_p^*: (□) left side; (■) right side.

Vortical-structures visualization

Laser tomography images allow revealing the structuring of the seeded jet and the surrounding air. In the presence of the flame the seeding droplets evaporate at the isotherm giving the flame front aspect at that temperature. Convective structures, such as vortices, are clearly noted. Under the action of the two types of longitudinal modes the vortical structures both form in the outer (and inner) layer and develop similarly; as a consequence they identically impact the flame front.

Fig. 10 illustrates such an example for case A. A vortex pairing process without merging occurs. This leads to two kinds of successive vortices, labeled V1 and V2, which was previously identified in [1] with the longitudinal mode induced by a transverse wave. If their formation is identical, they evolve in a different manner during their convection. V1 remains large and rather circular, and keeps a quite strong vorticity, while V2 is rapidly stretched and loses its vorticity (see the following sections for their dynamical properties). V1 and V2 are found here for both the direct and induced longitudinal mode with the same characteristics. These elements give a first evidence of a similar flame dynamics

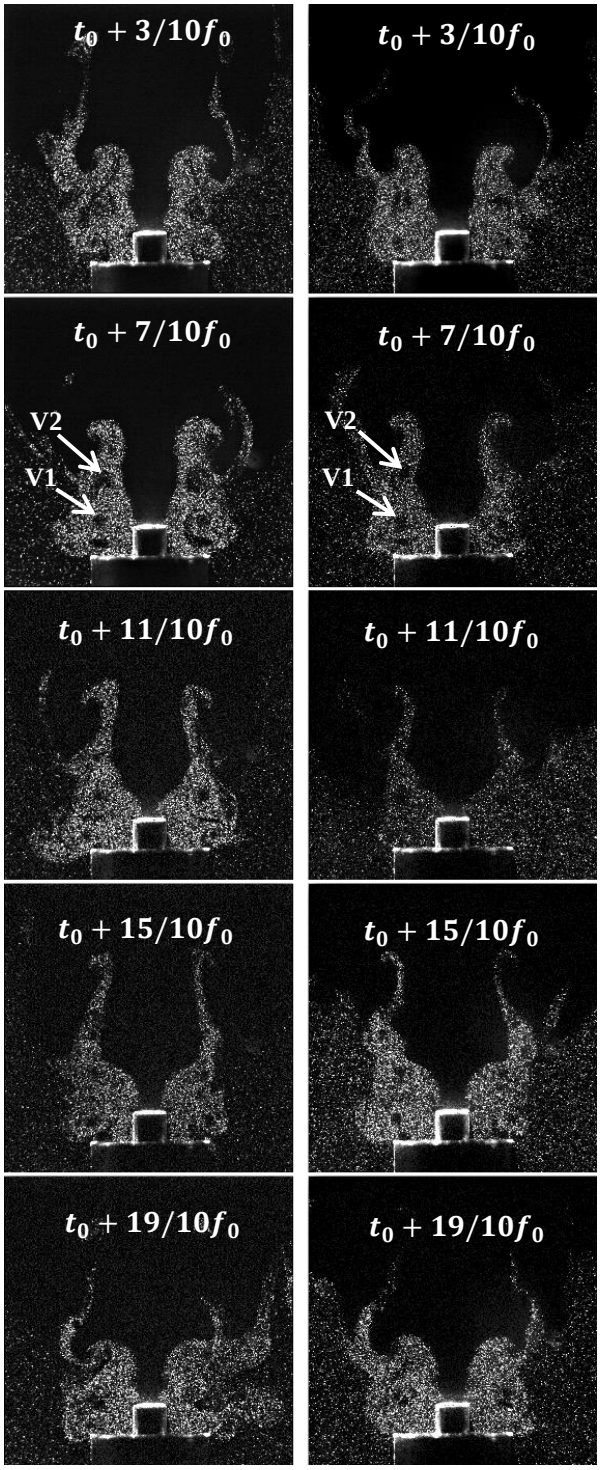

Fig. 10. Seeded jet-flow and surrounding air visualization. **Left:** direct longitudinal mode. **Right:** Induced longitudinal mode. Case A.

response behavior, verified then by means of the analysis of spectral energy of the CH* emission signal.

Flow field properties

In order to characterize the flow field nature, a velocity transfer function (VTF) of the aerodynamic field calculated at a frequency f is defined as the ratio of the amplitude of a current vertical or radial velocity compo-

nent ($U'_{p,max}$ or $V'_{p,max}$) measured at a point (x, y, z) over the one measured at the burner exit ($x, y, z_0 =$ 0.21 mm). Here the VTF is calculated on one hand from the center of the annular section of the burner exit ($x = \pm 3{,}25$ mm, $y = 0$) and on the other hand from its edge ($x = \pm 5$ mm, $y = 0$) up to the flame front along the associated vertical lines. The evolution of the VTF gain and phase φ along z leads to interpret the velocity field as the superposition of a convective perturbation and an acoustic one. For each studied case, both VTF properties evolve in a same manner. An example is given in Fig. 11 where the VTF for $x = \pm 3.25$ mm is calculated for $U'_{p,max}(f, z)$ in the case A characterized by the frequency bifurcation phenomenon both for f_0 (□) and $f_0/2$ (Δ). It has been chosen to report $U'_{p,max}$ rather than the gain $U'_{p,max}(f, z)/U'_{p,max}(f, z_0)$.

The evolutions of the VTF parameters, $U'_{p,max}$ and φ are the same in the two types of acoustic forcing, as reported in Fig. 11a and 11b. They are well described by the following relationships (eq. 2), which correspond to red continuous lines in Fig. 11b:

$$U'_p = U'_{p,ac} + U'_{p,cv} \quad (2)$$

with: $U'_{p,ac} = A_{ac}\exp(a_{ac}z)\exp(ik_{ac} - i2\pi ft + i\varphi_{ac})$

$U'_{p,cv} = A_{cv}\exp(a_{cv}z)\exp(ik_{cv} - i2\pi ft + i\varphi_{cv})$

A_{ac} and A_{cv} are the amplitudes of the acoustic and the convective perturbations respectively. The spatial damping coefficient of the acoustic and convective perturbation are a_{ac} and a_{cv} respectively. The acoustic wave number k_{ac} can be considered null; the convective wave number k_{cv} is defined as the ratio $2\pi f/U_{cv}$where U_{cv} is a mean convective velocity (see [8]).

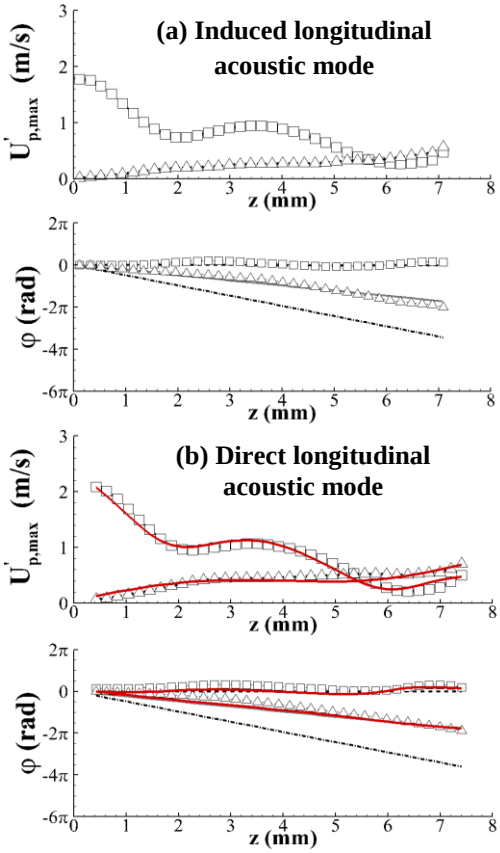

Fig. 11. Transfer functions of the vertical velocity U'_p at $x = \pm 3.25$ mm for f_0 (□) and $f_0/2$ (Δ). Up: velocity amplitude $U'_{p,max}$; down: phase φ . Case A.

The vorticity $\vec{\omega} = \vec{\nabla} \wedge \vec{v}$ is calculated in the plane y=0 as $\vec{\Omega} = (\vec{\omega} \wedge \vec{e}_y)\vec{e}_y$. The vortices produced in the outer layer due to the jet adaptation to the pressure field modulation have the same properties during all the formation and development: trajectory, shape, vorticity intensity, mutual interaction when it exists for all the cases. This is illustrated for the case A. From PIV images (e.g. in Fig. 12) vortices V1 and V2 are identified at the same position at the same time during a cycle for both acoustic modes. Their trajectories obtained by following the vortex center over time are reported in Fig. 13. After an identical formation (FZ), V1 and V2 develop differently in the convention zone (CZ), induced by the pairing process. V2 rapidly disappears due to a loss of its vorticity intensity (VD zone) while V1 attains the flame front and impacts it (FI).

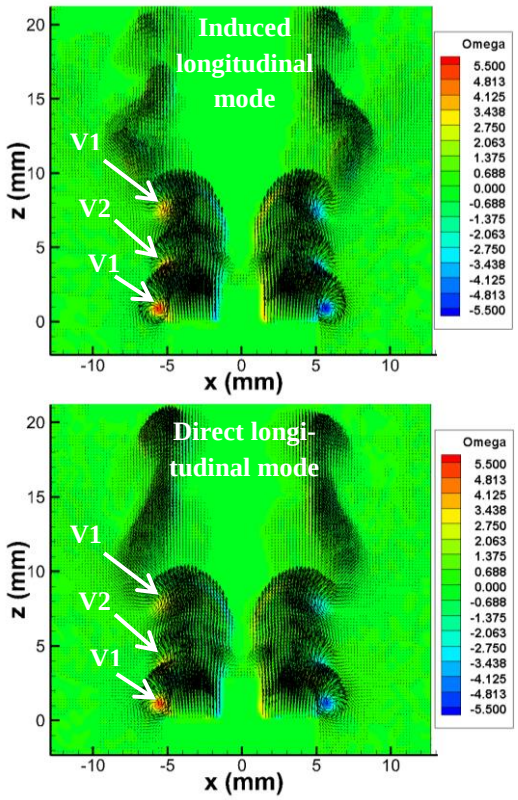

Fig. 12. Velocity and vorticity fields from PIV at $t_0 + 19/10f_0$. Case A

Flame dynamics

The analysis of the CH* emission signal $I_{CH^*}(t)$ shows the same energy spectrum characteristics for the two modes configurations. This is exemplified for case A in figure 14. Each spectrum presents two peaks: one at the forcing frequency f_0 and the other one at the sub-harmonic$f_0/2$. The detection of $f_0/2$ results

from the impact of successive vortices V1 and V2 on the flame front which impose a flame surface variation

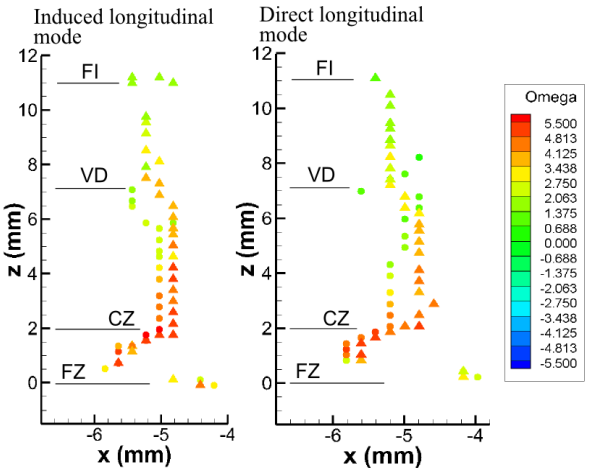

Figure 13. V1 (Δ) and V2 (∘) trajectories for case A in Table 1: FZ, formation zone; CZ, convection zone; VD, vorticity disappearance; FI, flame impact.

at $f_0/2$ by alternately rolling up and stretching the flame. The detection of f_0 comes from the flame foot displacement which is always modulated at the forcing frequency; this latter one is able to generate vortices in

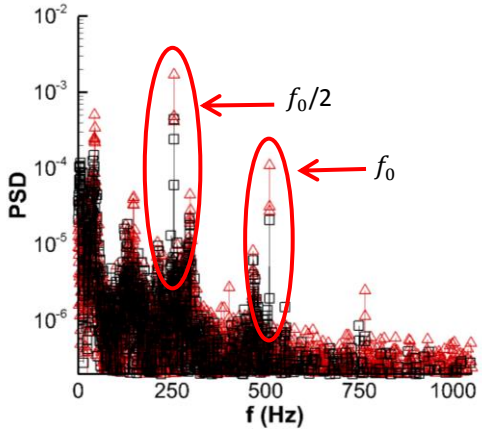

Fig. 14. PSDs of CH* emission signal for both transverse Δ and direct longitudinal modes □

the inner layer which participate in the flame surface modulation [9]. As the global CH* emission varies, the heat release rate fluctuates, mainly at $f_0/2$ with the persistence of f_0 [8]. It shows the frequency bifurcation in the flame dynamics response, previously described in [1].

Conclusions

Two configurations corresponding to typical chamber acoustic modes have been compared: (i) a direct longitudinal mode that generates a pressure pumping phenomenon. It is obtained via jet oscillations produced by a loudspeaker mounted at the burner bottom; (ii) a transverse mode that leads to a pressure plugging phenomenon, inducing a longitudinal mode in the burner. The burner has been placed at the wave pressure antinode where the induced longitudinal mode is maximum and undisturbed by phenomena which occur at other locations of the transverse acoustic field. For the plugging effect the acoustic pressure and jet acceleration are globally out-of-phase while for the pumping effect the acoustic pressure and jet acceleration are globally in-phase. Even though the plugging mechanism is opposed to the pumping one, they lead to the same dynamics properties of the jet and flame. Analysis of those properties clearly demonstrates that the induced longitudinal mode is identical to the direct longitudinal mode.

References

[1] F. Baillot, F. Lespinasse. Combust. Flame 161 (5) (2014) 1247-1267.

[2] Jean-François Bourgouin. Dynamique de flamme dans les foyers annulaires comportant des injecteurs multiples, PhD thesis, École Centrale Paris, 2014.

[3] J. O'Connor, T. Lieuwen, J. Eng. Gas Turbines Power (134) (2012) 1-9.

[4] G. Staffelbach, L. Gicquel, G. Boudier, T. Poinsot. Proc. Combust. Inst. 32 (2) (2009) 2909-2916.

[5] V. Yang, W. Anderson, Liquid rocket engine combustion instability, Progress in Astronautics and Aeronautics, vol. 169, AIAA Publications, Washington, DC 1995.

[6] F. Lespinasse, F. Baillot, T. Boushaki, C. R. Mec.341 (2013) 110-120.

[7] S. Candel, S. Ducruix, T. Schuller, D. Durox, F. Lacas. in: 5th Symp. on Smart Control of Turbulence (2004) 1-20.

[8] Florian Lespinasse. Réponse de la dynamique d'une flamme prémélangée à des modes acoustiques transverses, PhD thesis, Normandie University 2014.

[9] A. Cuquel, D. Durox, and T. Schuller. C. R. Mec. 341 (1-2) (2013) 171-180.